Carbon Monoxide Adducts of KatG and KatG(S315T) as Probes of the Heme Site and Isoniazid Binding†

Gudrun S. Lukat-Rodgers,‡ Nancy L. Wengenack,§ Frank Rusnak,§ and Kenton R. Rodgers*,‡

Department of Chemistry, North Dakota State University, Fargo, North Dakota 58105, and Hematology Research, Department of Biochemistry and Molecular Biology, Mayo Clinic and Foundation, Rochester, Minnesota 55905

Received February 21, 2001; Revised Manuscript Received April 26, 2001

ABSTRACT: KatG, the catalase peroxidase from *Mycobacterium tuberculosis*, is important in the activation of the antitubercular drug, isoniazid. About 50% of isoniazid-resistant clinical isolates contain a mutation in KatG wherein the serine at position 315 is substituted with threonine, KatG(S315T). The heme pockets of KatG and KatG(S315T) and their interactions with isoniazid are probed using resonance Raman (rR) spectroscopy to characterize their ferrous CO complexes. Three vibrational modes, C−O and Fe−C stretching and Fe−CO bending, are assigned using ^{12}CO and ^{13}CO isotope shifts. Two conformers are observed for KatG−CO and KatG(S315T)−CO. Resonance Raman features assigned to form I are consistent with it having a neutral proximal histidine ligand and the Fe−C−O moiety hydrogen bonded to a distal residue. The ν(C−O) band for form I is sharp, consistent with a conformationally homogeneous Fe−CO unit. Form II also has a neutral proximal histidine ligand but is not hydrogen bonded. This appears to result in a conformationally disordered Fe−CO unit, as evidenced by a comparatively broad C−O stretching band. The ^{13}CO-sensitive bands assigned to form II are predominant in the KatG(S315T)−CO rR spectrum. Isoniazid binding is apparent from the resonance Raman signatures of both WT KatG−CO and KatG(S315T)−CO. Moreover, isoniazid binding elicits an increase in the form I population of wild-type KatG−CO while having little, if any, effect on the already low population of form I of KatG-(S315T)−CO. Since oxyKatG (compound III) also contains a low-spin diatomic ligand−heme adduct (heme−O_2), it is reasonable to suggest that it too would exist as a mixture of conformers. Because the small form I population of KatG(S315T)−CO correlates with its inability to activate INH, we hypothesize that form I plays a role in INH activation.

Mycobacterium tuberculosis (*Mtb*)[1] infection is the second largest worldwide killer among infectious diseases, topped only by HIV/AIDS (*1*). Current treatment for tuberculosis (TB) involves daily therapy over the course of several months with the first-line drugs, isoniazid (isonicotinic acid hydrazide, INH), rifampin (RIF), pyrazinamide, and ethambutol (*2*−*4*). In the United States, 13% of all new TB cases are resistant to at least one of the first-line drugs; 1.6% of the cases are resistant to both INH and RIF (*5*). In INH-sensitive strains of *Mtb*, INH is rapidly converted into isonicotinic acid, isonicotinamide, pyridine-4-carboxaldehyde, and 4-pyridylmethanol (*6*, *7*). INH activation results in inhibition of mycolic acid synthesis in mycobacteria. Mycolic acids, long-chain (C_{70}−C_{90}) α-branched, β-hydroxy fatty acids, are building blocks of the mycobacterial cell wall. Two enzymes involved in mycolic acid synthesis, InhA (NADH-dependent enoyl-ACP reductase) and KasA (β-ketoacyl ACP synthase), are inhibited by a metabolite of INH (*9*−*11*) that is generated by functional KatG (*8*, *12*−*15*). The hypothesis that INH is a prodrug, whose activation in vivo is dependent on KatG, has been reinforced by chemical and structural characterization of an INH adduct, isonicotinic acyl-NADH, bound at the active site of InhA (*16*, *17*).

Studies of clinical isolates have shown that 50−70% of INH-resistant strains are mutated at the *katG* locus with missense mutations (rather than gene deletion) being the most common alteration (*18*−*21*). The most frequent *katG* mutation found in INH-resistant strains results in amino acid substitutions at Ser315 of KatG, with S315T being the most common (*19*, *22*, *23*). INH sensitivity is restored to INH-resistant *Mtb* strains by introduction of functional, plasmid-borne *katG* (*24*, *25*). Hence, INH sensitivity is modulated, at least in part, by *Mtb* KatG. The structural and conformational origin(s) of compromised INH activation by mutant KatGs and the role(s) played by mutation remain(s) a mystery.

The *Mtb katG* gene encodes a heme-containing catalase−peroxidase which has significant sequence homology with a superfamily of plant, fungal, and bacterial catalase/peroxidases.

† This work was supported by NIH Grant AI41217-01 (G.S.L.-R.), USDA Grant 97-35305-5158 (K.R.R.), Hermann Frasch Foundation Grant 446-HF97 (K.R.R.), and the Mayo Foundation (F.R.).

* To whom correspondence should be addressed. Telephone: (701) 231-8746. Fax: (701) 231-8831. E-mail: Kent_Rodgers@ndsu.nodak.edu.

‡ North Dakota State University.

§ Mayo Clinic and Foundation.

[1] Abbreviations: *Mtb*, *Mycobacterium tuberculosis*; WT, wild type; 6-c, six coordinate; 5-c, five coordinate; LS, low spin; HS, high spin; rR, resonance Raman; ESR, electron spin resonance; INH, isonicotinic acid hydrazide; δ(Fe−CO), Fe−C−O bending vibrational mode; HRP, horseradish peroxidase; ν(Fe−CO), Fe−C stretching vibrational mode; CCP, cytochrome *c* peroxidase; ν(C−O), C−O stretching vibrational mode; TB, tuberculosis.

10.1021/bi010369g CCC: $20.00
Published on Web 05/25/2001

Sequence alignment of KatG with *Saccharomyce cerevisiae* cytochrome *c* peroxidase (CCP) suggests that Ser315 is analogous to Ser185 in CCP, which is part of the heme pocket and participates in hydrogen bonding with a heme propionate group (*19*, *26*). Several properties of KatG are relatively unperturbed by the S315T substitution. The heme redox potential ranges only from −21 to −77 mV vs NHE for wild-type (WT) KatG and KatG(S315T) in the presence and absence of INH (*27*). Wild-type KatG and KatG(S315T) proteins are both competent catalase−peroxidase enzymes with comparable catalase and peroxidase activities (*28*, *29*). Hence, compounds I and II are both accessible in the WT and (S315T) enzymes. Compound I was recently observed spectroscopically after treatment of WT KatG with *tert*-butyl hydroperoxide and percarboxylic acids (*30*). Compound I for KatG(S315T) was not reported. INH binds near the heme in both enzymes, as evidenced by NMR relaxation results from which the Fe−INH amide nitrogen distance was estimated at ∼4 Å for both proteins [WT KatG−INH (3.8 ± 0.8 Å) and KatG(S315T)−INH (4.4 ± 0.9 Å)] (*32*).

Nevertheless, *Mtb* strains carrying the *katG(S315T)* mutation are INH resistant because of their inability to activate INH. There are differences in the heme environments of WT KatG and KatG(S315T) that manifest themselves as subtle perturbations in the spectroscopic signatures of the heme. Low-temperature ESR spectra reveal slight changes in the five-coordinate (5-c) and six-coordinate (6-c) populations of high-spin (HS) ferric WT and KatG(S315T) hemes upon addition of INH, further suggesting that INH binds near the heme iron in both enzymes (*33*). UV−visible (*33*, *34*) and resonance Raman (rR) (*34*) data suggest that the distal heme environment of ferric and ferrous KatG(S315T) is altered relative to WT KatG as demonstrated by a greater population of 6-c low-spin (LS) heme in KatG(S315T) relative to WT KatG under typical INH assay conditions. In addition to these spectroscopic signatures, KatG has been observed to form a superoxide complex (compound III) that is more reactive than that for HRP (*30*, *35*). Moreover, KatG(S315T) is less efficient at converting INH to isonicotonic acid via a mechanism involving superoxide (*31*). The rate constant for INH oxidation catalyzed by KatG(S315T) is 7−11 times smaller than for WT KatG (*28*, *31*).

A full understanding of the reactivity of bound O_2 toward INH could shed light on the reason(s) for the inability of KatG(S315T) to activate INH. The structural and electronic factors that govern the reactivity can be reported by the vibrational modes of the bound diatomic ligand. While O_2 adducts of peroxidases are reactive, CO and NO form thermodynamically stable adducts with ferrous peroxidases that can be probed by spectroscopic techniques. Indeed CO− and NO−peroxidase complexes have been extensively studied, and the structural information inferred from their vibrations has contributed to understanding the structural basis of their catalytic activities (*36*−*46*). Vibrational signatures of three diatomic ligand complexes are commonly exploited as probes of distal heme environment. They are the ferric and ferrous heme−CN, ferrous heme−NO, and ferrous heme−CO adducts. Each has its own advantages and limitations for probing distal pocket properties. The minimal π back-bonding in heme−CN adducts (*47*, *48*) allows substantial conformational flexibility in the Fe−C−N moiety. Hence, the Fe−CN unit is easily bent and/or tilted under the influence of distal steric interactions and provides insight into them (*49*). The dispersion in ν(C−N) frequencies is small across the heme proteins and is rather insensitive to electrostatic interactions (*49*). The ferrous heme−NO adducts fall into 5-c and 6-c categories. The heme−NO adducts are arguably the best mimics of their O_2 counterparts for two reasons. First, both have bent Fe−X−O equilibrium geometries. Second, both show little dependence of Fe−X distance on the presence or absence of a proximal ligand. Because of this domination of the d_{z^2} σ bonding by overlap with the occupied nonbonding orbitals of NO and O_2, both their 5-c and 6-c adducts fall on the same ν(Fe−X)/ν(X−O) correlation line. Although recent studies have demonstrated the utility of back-bonding correlations for NO and O_2 adducts of ferrous hemes and model complexes (*50*), these correlations provide little insight into proximal endogenous ligand bonding.

In this study, CO has been chosen as the ligand probe, as it yields insight into important structural and electronic properties of both proximal and distal heme environments. This steady-state rR investigation of ferrous heme−CO adducts allows comparison of the distal and proximal heme pocket influences on the Fe−C−O units of WT KatG−CO and KatG(S315T)−CO. The effect of INH on these vibrations in the WT and KatG(S315T) proteins is also reported. Characterization of the distal heme pocket via its interactions with these stable heme−CO adducts is providing initial insights into the interactions that could govern structure and reactivity of a heme-bound O_2 ligand.

MATERIALS AND METHODS

Protein Isolation and Sample Preparation. Mtb WT KatG and KatG(S315T) proteins were overexpressed and purified from *Escherichia coli* using the previously reported protocol (*28*). Protein concentrations were determined using the Bradford assay with bovine serum albumin as the standard (*51*). All WT KatG and KatG(S315T) samples were in 50 mM sodium phosphate at pH 7.5 or in 50 mM Tris-HCl at pH 7.8 and 8.0. Ferric samples were flushed extensively with N_2 prior to addition of INH to prevent catalytic turnover.

Reduced WT KatG− and KatG(S315T)−CO adducts were prepared anaerobically by reducing ferric proteins with a 10−20-fold excess of sodium dithionite (buffered 0.1 M sodium dithionite solution) followed by equilibration with 1 atm of ^{12}CO (natural abundance) or ^{13}CO (99% ^{13}C). Carbonyl adduct formation was confirmed by UV−visible spectroscopy. UV−visible spectra were recorded at ambient temperature on a CCD-based multichannel spectrometer under microcomputer control. Isoniazid stock solutions (10−300 mM) were prepared anaerobically with recrystallized INH immediately before use. Buffers used for pH dependence of Fe−CO stretching bands were citrate (pH 4.5), phosphate (pH 6.0), MOPS (pH 7.0), Tris (pH 8.0), and glycine (pH 1.0); buffer concentrations were 50 mM.

Resonance Raman Spectroscopy. Resonance Raman spectra were obtained with either 406.7 or 413.1 nm excitation from a Kr^+ laser via backscattering from 0.1 to 0.3 mM KatG samples. Samples were in 5 mm NMR tubes spun at approximately 20 Hz at ambient temperature. Laser powers were between 0.2 and 20 mW at the sample, and spectral artifacts due to photoinduced chemistry were avoided by

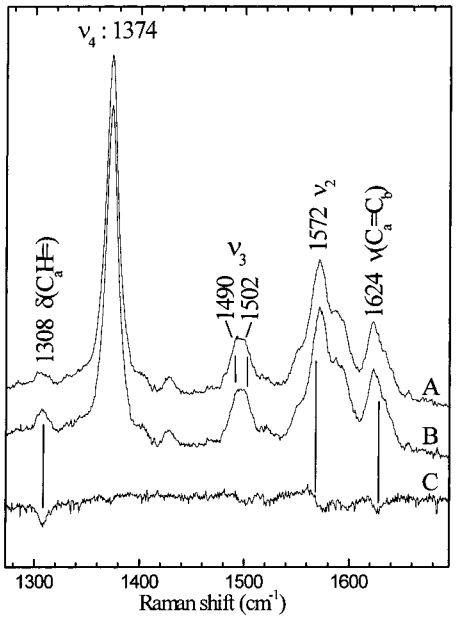

FIGURE 1: High-frequency resonance Raman spectrum of ferric WT KatG with 406.7 nm excitation: (A) 320 μM WT KatG in 50 mM Tris-HCl, pH 8.0, (B) 320 μM WT KatG plus 5 equiv of INH in 50 mM Tris-HCl, pH 8.0, and (C) difference spectrum [(WT KatG) − (WT KatG/INH)] in 50 mM Tris-/HCl, pH 8.0 (spectrum A − spectrum B). The difference spectrum is multiplied by a factor of 2. Laser power at the sample was 10 mW.

judicious control of the incident power. Spectra were recorded with a Raman spectrometer described previously (*34*). The spectrometer was calibrated with neat toluene, DMF, CCl_4, CH_2Br_2, and DMSO as frequency standards. UV−visible spectra were obtained before and after rR experiments to ensure that the samples were not irreversibly altered in the laser beam. For the CO adducts, the ν_4 mode region was examined for evidence of CO photolysis. At powers between 5 and 20 mW at the sample, the amount of 5-c ferrous heme present due to laser photolysis of the CO, as judged by ν_4 intensity at 1355 cm^{-1}, was not significant and, therefore, not likely to contribute to the rR spectra in the low-frequency region. To avoid introduction of artifacts in the rR difference spectra, baselines were either left uncorrected or simply offset by subtraction of a straight line from the spectrum.

ESR Spectroscopy. For ferric forms of the KatG proteins, ESR spectra were recorded at 15 K with a spectrometer operating at X-band microwave frequency (9.45 GHz) and equipped with an continuous flow helium cryostat. At a microwave power of 2 mW, neither the LS nor HS components of the spectra were saturated.

RESULTS

Ferric KatG and KatG(S315T) Interactions with INH. Optical difference spectra of WT KatG titrated with INH show a small blue shift in the Soret band maximum from 408 to 406 nm (*33*). This result and ESR studies are consistent with an INH-induced change in coordination number from 6-c to 5-c (*33*). To further examine the effects of INH binding to WT KatG, its high-frequency rR spectrum was monitored as the enzyme was titrated with INH at room temperature. Curves A and B in Figure 1 show the 406.7 nm excited rR spectra obtained from ferric WT KatG upon treatment with INH. In this spectrum, one of the core-size marker bands, ν_3, is particularly sensitive to heme spin state and coordination number. In the difference spectrum (WT KatG − WT KatG/INH) (Figure 1C), there is a small difference feature at 1486/1499 cm^{-1} corresponding to a shift in the ν_3 band, indicative of a change in coordination number of a small fraction of the WT KatG heme from 6-c HS to 5-c HS (*52*). Evidence suggests that water is the sixth ligand in 6-c HS WT KatG (*33*, *34*). Conversion of a 6-c HS heme to a 5-c HS heme suggests that INH binding may promote changes in the distal pocket that include loss of coordinated water. These assignments were made by analogy to metMb (*53*). To confirm that these small difference features were not artifacts of the subtraction process, the difference spectrum [(WT KatG, sodium phosphate, pH 7.5) − (WT KatG, Tris-HCl, pH 8.0)] (not shown) was examined, and no difference features were observed. The same subtle spectral changes were observed when INH treatment was carried out in sodium phosphate at pH 7.5 or in Tris-HCl at pH 8.0 with 6 or 70 equiv of INH, respectively. Even though these difference features are reproducible and do not vary with incident laser power (0.8−15 mW at sample), they are all small, suggesting that the fraction of protein being interconverted in response to INH binding is also small. Hence, these data indicate that INH binding does not cause a large shift in the WT KatG spin state or coordination state populations in solution at room temperature.

Larger INH-induced difference bands were observed for ν_2 and the vinyl modes, $\nu(C_a{=}C_b)$ and $\delta(C_aH{=})$. Notably, two of these, ($\delta(C_aH{=})$ and $\nu(C_a{=}C_b)$, are directly associated with the vinyl substituents. These vinyl coordinates can mix with skeletal modes, including ν_2 (*45*, *54*). This may explain why the largest difference feature occurs at the ν_2 frequency. Although changes in mixing of vinyl and porphine skeletal coordinates can be associated with a coordination state change, given the relative insensitivity of ν_3 to INH interaction, it is more likely that they occur in response to perturbations of the peripheral heme environment in response to INH binding.

When INH binding to ferric WT KatG is monitored by low-temperature ESR, as shown in Figure 2, shifts in the distribution of species are also observed. The ESR spectrum of WT KatG contains signatures from three HS species (*33*) and multiple 6-c LS species (*34*). The effect of INH on the ESR spectra of KatG HS ferric species has been attributed to INH-induced changes in the relative populations of axial and rhombic species (*33*). The ESR spectra in Figure 2 reveal that addition of INH also results in the loss of a prominent 6-c LS species ($g = 3.24, 2.05, 1.28$). Due to the overlapping ESR signals, species quantitation is nontrivial. However, the increase in relative intensity at $g \approx 6$ suggests that this 6-c LS species is converted to a HS species in the presence of INH. This conversion is more apparent in the 15 K ESR spectra than in their room temperature rR counterparts because at 15 K a larger fraction of WT KatG is 6-c and LS, whereas it is predominantly HS at room temperature (*34*). INH-induced changes in the ESR signatures of both HS and LS species involve alteration in distal heme coordination, suggesting INH binding affects the distal environment of the heme.

Like WT KatG, ferric KatG(S315T) exhibits HS and LS forms in its ESR spectrum (*33*, *34*). The previously reported

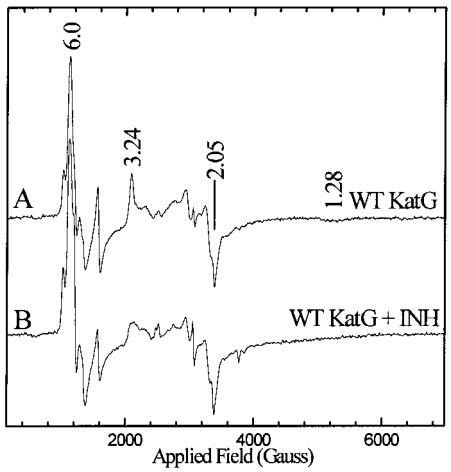

FIGURE 2: Effect of INH on the electron spin resonance spectrum of ferric WT KatG: (A) WT KatG; (B) WT KatG with 2 equiv of INH. Samples were in 50 mM Tris-HCl, pH 7.8. Instrument parameters: 15 K, 2 mW, 10.4 G modulation amplitude at 100 kHz modulation frequency, 9.454 GHz, 164 ms time constant, and 7000 G sweep width.

ESR spectrum of recombinant ferric KatG(S315T) (*34*) is not detectably altered by addition of INH (data not shown). This is not all together surprising, since titration with INH does not significantly alter the visible spectrum of recombinant KatG(S315T) (*33*). This study exploits spectroscopic signatures of heme-bound CO to probe the heme environment as a means of elucidating the differential effects of INH on WT KatG and KatG(S315T).

Heme−CO Vibrations as Probes of Heme Environment in WT KatG−CO and KatG(S315T)−CO. To probe the S315T mutation- and INH-induced changes in the distal heme pocket of KatG, where both INH and oxidizing agents such as H_2O_2 and O_2 interact with the heme, we have undertaken a study of the KatG−CO adducts. The visible spectra of the ferrous CO adducts of WT KatG and KatG(S315T) indicate they are typical 6-c LS complexes with a proximal histidine ligand (inset, Figure 3). The visible spectrum of WT *Mtb* KatG−CO with a 422 nm Soret and α/β bands at 572/542 nm is comparable to that previously reported for *Mycobacterium smegmatis* KatG−CO (55). The band maxima for KatG(S315T)−CO are slightly shifted (421 nm Soret; 570/540 nm α/β bands). Occurrence of ν_4 at 1372 cm^{-1} in the high-frequency rR spectra of WT KatG−CO and KatG(S315T)−CO (Figure 3) is also typical for heme−CO adducts (*38*). The lack of a shoulder near 1358 cm^{-1} [ν_4 for 5-c HS Fe(II)] indicates that a 5-c photoproduct is not produced in significant amounts during Raman excitation. The ν_4 and other heme skeletal vibrations were unaffected by addition of INH to either WT KatG−CO or KatG(S315T)−CO (data not shown).

The Fe−CO vibrations of heme−CO adducts are exquisitely sensitive to modes of interaction between the distal pocket and bound CO. This sensitivity derives from the influence of distal electrostatic and steric factors on the extent of Fe → CO π back-bonding, which has the effect of increasing the Fe−C bond order and decreasing the C−O bond order. Raman bands due to vibrations of WT KatG−CO involving the heme CO ligand were identified on the basis of isotope shifts for the ^{13}CO isotopomer. Isotope-sensitive bands in the rR spectrum of WT

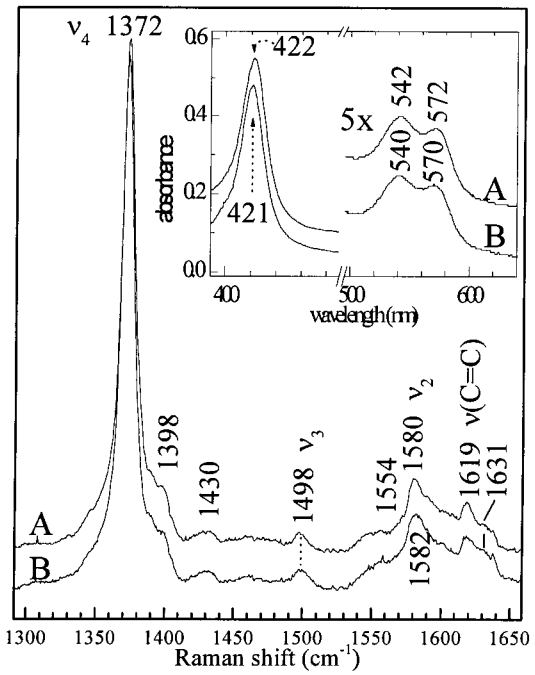

FIGURE 3: High-frequency resonance Raman spectrum of KatG CO adducts: (A) WT KatG−CO (220 μM); (B) KatG(S315T)−CO (154 μM). The samples were in 50 mM Tris-HCl, pH 7.8, with a 20-fold excess of sodium dithionite and 1 atm of CO. Spectra were obtained with 413.1 nm excitation and 0.4 mW laser power at the sample. Inset: Visible absorbance spectra of the KatG−CO adducts: (A) WT KatG−CO; (B) KatG(S315T)−CO. Spectra are vertically offset from one another on the same absorbance scale. Both samples were 9.0 μM in heme, were in 50 mM Tris-HCl at pH 7.8, contained a 4-fold excess of sodium dithionite, and were under 1 atm of CO.

KatG−CO are shown in Figure 4. In the WT KatG−^{12}CO spectrum, the bands at 499 and 522 cm^{-1} are assigned to Fe−CO stretching vibrations [ν(Fe−CO)] due to two different conformations of the Fe−CO unit, form I and form II. The ν(Fe−CO) bands shift to 495 and 516 cm^{-1}, respectively, in the WT KatG−^{13}CO spectrum. A Fe−C−O bending mode [δ(Fe−C−O)] occurs at 584 cm^{-1}. In the ^{13}CO isotopomer, this bending mode shifts to 568 cm^{-1}. The two CO stretching bands, ν(C−O), at 1926 and 1965 cm^{-1} were also assigned by isotopic substitution. The 1926 cm^{-1} band is sharp and readily observed in the high-frequency spectrum. It shifts to 1886 cm^{-1} upon ^{13}CO substitution, which is the isotope shift predicted for a diatomic CO oscillator. Since the resonance enhancement is poor for the high-frequency C−O stretching region of the rR spectrum, and since the pixel to pixel response variation of the detector approaches the intensities of weak ν(C−O) bands, it is difficult to observe weak, broad bands in this region of the spectrum. Therefore, the second ν(C−O) band at 1965 cm^{-1}, which is quite broad, is clearly visualized only in the difference spectrum (Figure 4C) after the pixel response artifacts are canceled by subtraction of the KatG−^{13}CO spectrum. The 1965 cm^{-1} band shifts to around 1918 ± 4 cm^{-1} upon ^{13}CO substitution. The negative component for the ^{13}CO isotopomer in the difference spectrum is superimposed on the positive feature of the 1926 cm^{-1} band, making exact assignment of the^{13}C shift difficult. The 522 cm^{-1} ν(Fe−CO), 1926 cm^{-1} ν(C−O), and 584 cm^{-1} δ(Fe−C−O) bands are assigned to WT KatG−CO form I,

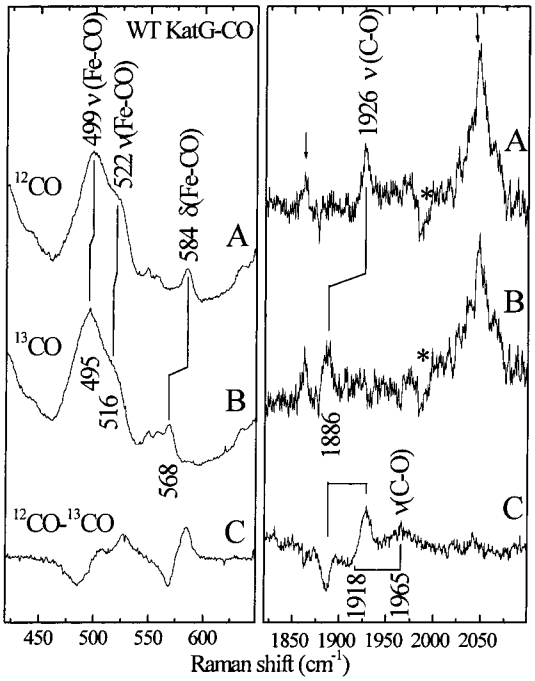

FIGURE 4: Resonance Raman spectra of WT KatG−CO: (A) WT KatG−^{12}CO; (B) WT KatG−^{13}CO; (C) difference spectrum of [(WT KatG−^{12}CO) − (WT KatG−^{13}CO)]. Samples were 220 μM in 50 mM Tris-HCl, pH 8.0. Spectra were obtained with 413.1 nm excitation with 10 mW laser power at the sample. The arrows indicate bands due to protein vibrations. The asterisk indicates a detector artifact, which is not observed in the difference spectrum because it is subtracted out with the protein bands.

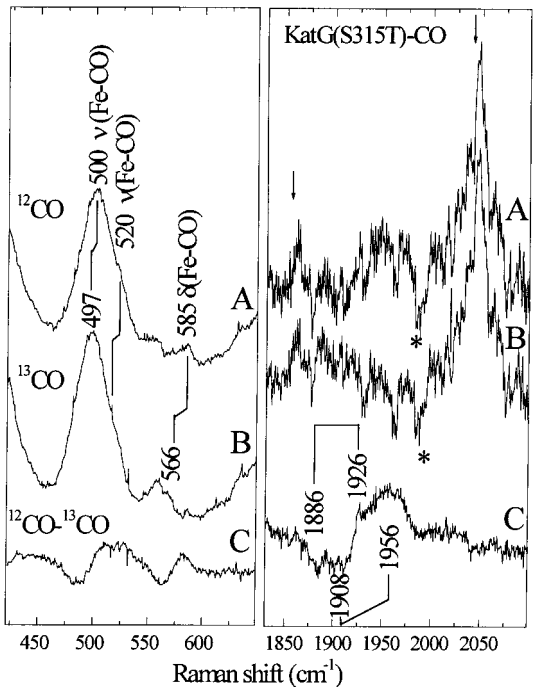

FIGURE 5: Resonance Raman spectra of KatG(S315T)−CO: (A) KatG(S315T)−^{12}CO; (B) KatG(S315T)−^{13}CO; (C) difference spectrum of [(KatG(S315T)−^{12}CO) − (KatG(S315T)−^{13}CO)]. Samples were 200 μM in 50 mM Tris-HCl, pH 8.0. Spectra were obtained with 413.1 nm excitation with 10 mW laser power at the sample. The arrows indicate bands due to protein vibrations. The asterisk indicates a detector artifact. The detector artifact is not observed in the difference spectrum because it is subtracted out with the protein bands.

while form II exhibits ν(Fe−CO) at 499 cm^{-1} and ν(C−O) at 1965 cm^{-1}. Band assignments to forms I and II are based on mutual interchanges of intensity between these bands in the KatG(S315T)−CO spectrum (vide infra) and by analogy to other peroxidases (*36*−*39*, *41*, *46*).

Vibrations involving the CO ligand in KatG(S315T)−CO were also assigned by isotopic substitution (Figure 5). Similar to WT KatG−CO, the Fe−CO stretching bands for KatG(S315T)−CO fall at 500 and 520 cm^{-1}, and the bend is at 585 cm^{-1}. Bands at 1926 and 1956 cm^{-1}, assigned to ν(C−O) for KatG(S315T)−^{12}CO, shift to 1885 and 1908 cm^{-1}, respectively, in the KatG(S315T)−^{13}CO spectrum. These spectra and the isotope difference spectrum (Figure 5C) clearly show that there are at least two Fe−CO conformations in KatG(S315T)−CO. The first Fe−CO conformation of KatG(S315T)−CO [520 cm^{-1} ν(Fe−CO), 585 cm^{-1} δ(Fe−C−O), 1926 cm^{-1} ν(C−O)] is the analogue of form I of WT KatG−CO. The 500 cm^{-1} ν(Fe−CO) and 1956 cm^{-1} ν(C−O) bands are assigned to an Fe−C−O conformation form II which is similar to its WT counterpart and appears to dominate the KatG(S315T)−CO spectrum. The assignments of sets of bands to forms I and II are based on the following two observations. First, the ν(Fe−CO) band at 520 cm^{-1} is associated with the bending vibration at 585 cm^{-1} because both are less intense relative to the 500 cm^{-1} band in the mutant. Second, the assignments of ν(Fe−CO) and ν(C−O) pairs to forms I and II in KatG(S315T)−CO were made so location of a point substantially above the imidazole π back-bonding correlation line (vide infra) was avoided. Placing a point above the imidazole correlation line would indicate a 5-c CO complex (*56*), which is inconsistent with our previously reported 6-c WT KatG−NO spectrum (*34*). Since NO is a stronger trans-labilizing ligand than CO, it is unlikely that the CO adduct would be 5-c in a protein whose NO adduct is 6-c.

The 520 and 585 cm^{-1} bands attributed to form I of KatG(S315T)−CO have lower relative intensities than their counterparts in the WT KatG−CO spectrum (Figure 4). This interchange in the populations of forms I and II is also apparent in the CO stretching region of the spectrum, as the sharp ν(C−O) band from form I is much less intense than it is in the WT KatG−CO spectrum (Figure 4C). Resonance Raman spectra of WT KatG−CO and KatG(S315T)−CO were recorded between pH 4.5 and pH 10 (data not shown.) Although no alkaline transitions were observed, both had similar populations of forms I and II at pH 4.5. However, loss of form I population was a steeper function of pH for the mutant than for the WT enzyme. This pH behavior and the intensity changes described above are consistent with form I being less stable in KatG(S315T)−CO.

Frequencies of the ν(Fe−CO) and ν(C−O) bands for heme−CO complexes are inversely correlated because of the aforementioned interplay between Fe → CO π back-bonding and population of CO-based π* molecular orbitals. Figure 6 shows this inverse correlation for a number of heme proteins. The height of a correlation line on the ν(Fe−CO) axis is biased by the σ donor strength of the trans (proximal) ligand. The inverse correlation between line height and proximal donor strength is due to competition between the CO and proximal ligand for the empty d_{z^2} orbital of the LS Fe(II) center. Hence, anionic proximal ligands such as imidazolate and thiolate lower the π back-bonding correlation

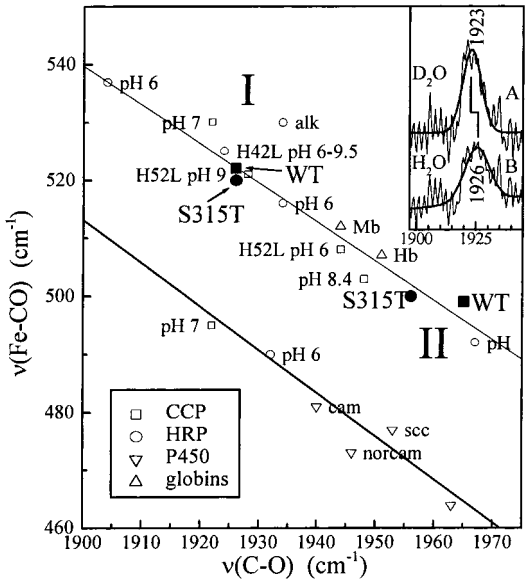

FIGURE 6: Plot of observed ν(Fe−CO) versus ν(C−O) frequencies for CO adducts of KatG. The back-bonding correlations for proximal imidazole ligation (top line) and for thiolate and imidazolate ligation (bottom line) are shown. Data for several carbonyl protein adducts under the conditions noted in the figure are shown: ■, WT KatG and WT KatG/INH (forms I and II for WT and WT/INH overlap); ●, KatG(S315T); □, CCP; ○, HRP; ▽, cytochrome P450; △, Mb and Hb. WT KatG and KatG(S315T) data are from this work while data for other CO adducts were taken from refs 34−44. The solid lines are linear least-squares fits of all the data points shown except those for the KatGs. The inset shows the 3 cm^{-1} downshift of the ν(C−O) band of form I when the spectrum is acquired from a D_2O solution of WT KatG−CO. Solid lines are least-squares fits using a Gaussian line shape.

line on the ν(Fe−CO) axis due to weakened Fe−CO σ bonding (*54*). For WT KatG−CO and KatG(S315T)−CO, forms I and II fall on the imidazole back-bonding line, consistent with proximal imidazole rather than imidazolate ligation in both Fe−CO forms for WT and mutant KatGs. This is in contrast to the two conformations observed for HRP−CO at pH 6.0 and CCP−CO at pH 7.0, where one conformation falls on the imidazole back-bonding line and the second on the imidazolate line (*36*−*39*, *41*, *46*).

The position of a point on a given correlation line reflects the degree of π back-bonding in the Fe−CO moiety, which is governed by both Fe−C−O geometry and the distal electrostatic field (*43*, *57*). An off-axis Fe−C−O geometry diminishes overlap of the CO-based π^* and d−π orbitals, resulting in weaker back-bonding and, absent electrostatic interactions such as hydrogen bonding, is characterized by positions to the right (low) on the correlation line. Interactions of the CO ligand with positively charged or H-bond-donating residues on the distal side of the heme are known to enhance π back-donation. Distal H-bond interactions are characterized by points high on the correlation line. Offsetting contributions from H-bonding and off-axis Fe−CO distortions tend to place points at intermediate positions on the plot in Figure 6. It has been suggested that points for Fe−CO units with ν(Fe−CO) > 520 cm^{-1} and ν(C−O) < 1935 cm^{-1} have distal H-bonds (*39*). Since form I falls close to this threshold, the ν(Fe−CO) frequency was measured in D_2O solution to determine whether it is indeed hydrogen bonded. The inset in Figure 6 shows the ν(Fe−CO) bands recorded in H_2O (top) and D_2O. A downshift is expected in D_2O if the bound

Table 1

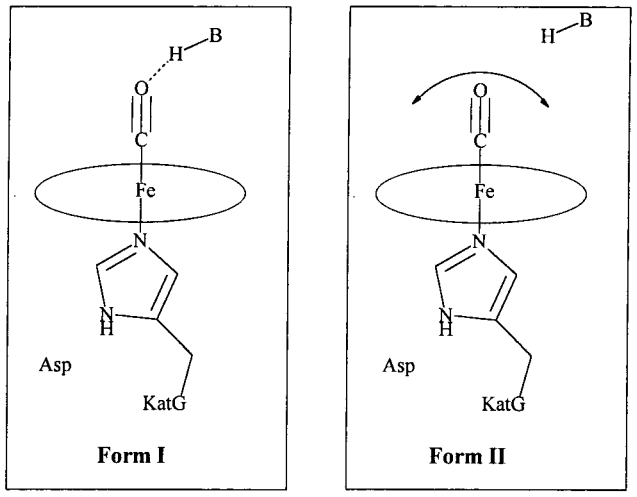

	form I		form II	
mode	WT	S315T	WT	S315T
ν(Fe−CO) (cm^{-1})	522	520	499	500
ν(C−O) (cm^{-1})	1926	1926	1965	1956
δ(Fe−C) (cm^{-1})	584	585		

CO is H-bonded to a donor with an exchangeable proton. The 3 cm^{-1} downshift in D_2O (Figure 6) is consistent with those previously observed for peroxidase−CO adducts with H-bonded CO ligands (*58*). Thus, forms I of WT KatG−CO and KatG(S315T)−CO contain Fe−CO moieties that are H-bonded to a distal residue. Form II for both enzymes falls much lower on the imidazole line than form I. By analogy to the high-pH form of CCP−CO with ν(Fe−CO), δ(Fe−CO), and ν(C−O) at 503, 575, and 1948 cm^{-1}, respectively (*39*), form II most likely contains a non-hydrogen-bonded Fe−CO unit. An Fe−C−O bending vibration cannot be assigned for form II. However, the possibility that forms I and II have nearly identical δ(Fe−C−O) frequencies cannot be eliminated. The breadth of the ν(C−O) band at 1956 cm^{-1} is consistent with a conformationally inhomogeneous Fe−CO unit in form II. The dominance of form II in the KatG(S315T)−CO spectrum further suggests that the S315T mutation alters the heme pocket such that the conformationally more flexible form II is favored. Table 1 shows the proposed Fe−CO conformations for WT KatG− and KatG(S315T)−CO adducts.

Interaction of WT KatG−CO and KatG(S315T)−CO with INH. The isotope-sensitive bands in the rR spectrum of WT KatG−CO/INH are shown in Figure 7. In the presence of INH, the two conformers of WT KatG−CO are also observed. The relatively intense δ(Fe−C−O) band at 584 cm^{-1} and the ν(Fe−CO) band at 522 cm^{-1} shift to 568 and 516 cm^{-1}, respectively, in the WT KatG−^{13}CO/INH spectrum and are assigned to the same Fe−CO conformation (form I). The second ν(Fe−CO) band occurs at 499 cm^{-1} with an apparent shift to 491 cm^{-1} in the ^{13}CO adduct. It is assigned to form II. The CO stretching vibrations are observed at 1926 and 1965 cm^{-1}. However, the relative intensity of the 1965 cm^{-1} band (form II) is diminished. This is consistent with the low-frequency spectrum in which the form II ν(Fe−CO) band loses intensity relative to the form I bending and stretching bands upon INH addition. Hence,

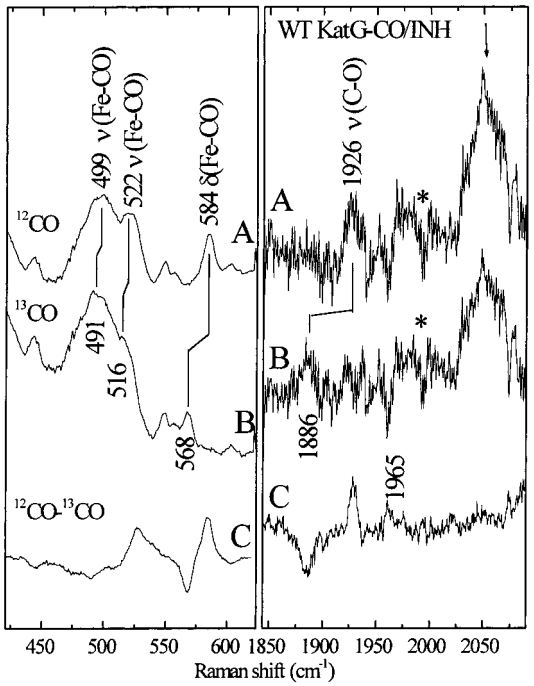

FIGURE 7: Resonance Raman spectra of WT KatG−CO/INH: (A) WT KatG−^{12}CO plus 70 equiv of INH; (B) WT KatG−^{13}CO plus 70 equiv of INH; (C) difference spectrum, (WT KatG−^{12}CO/INH) − (WT KatG−^{13}CO/INH) (spectrum A − spectrum B). The arrows indicate bands due to protein vibrations. The asterisk indicates a detector artifact.

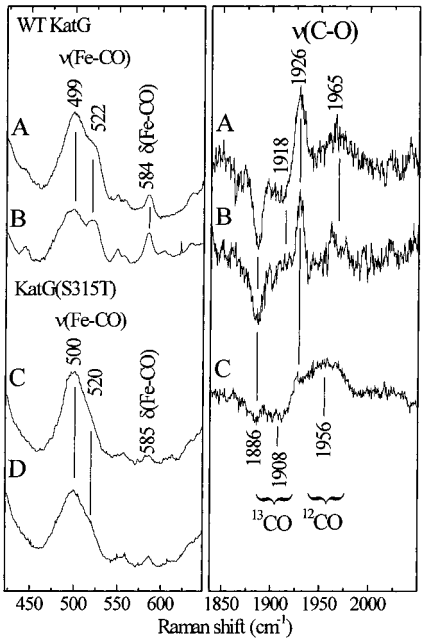

FIGURE 8: Effect of INH binding on the rR spectrum of WT KatG−CO and KatG(S315T)−CO: (A) WT KatG−CO; (B) WT KatG−CO plus 70 equiv of INH; (C) KatG(S315T)−CO; (D) KatG(S315T)−CO plus 70 equiv of INH. All samples were in 50 mM Tris-HCl, pH 8.0, and all spectra were obtained with 413.1 nm excitation using 10 mW laser power at the sample. High-frequency difference spectra (C−O stretching region) are those shown in Figures 4, 5, and 7.

the main effect of INH on WT KatG−CO is to shift the equilibrium between forms I and II in favor of form I, making the Fe−CO unit more conformationally homogeneous in WT KatG−CO.

To further examine the changes upon INH binding to CO adducts, rR spectra with and without INH are compared in Figure 8. Addition of INH to WT KatG−CO caused an intensity decrease of the 499 cm^{-1} ν(Fe−CO) band. In contrast to small shifts observed for HRP−CO upon substrate binding (*36*), no INH-induced shifts in the frequencies of the Fe−CO vibrations are observed for forms I or II of WT KatG−CO.

Treatment of KatG(S315T)−CO with INH causes a slight interchange in the intensities of the 500 and 520 cm^{-1} bands, suggesting that INH binds to the mutant enzyme but only slightly increases population of form I. We were unable to detect the ν(C−O) stretching band of KatG(S315T)−CO/INH. Since the ν(C−O) envelope is broad even prior to INH addition, it is possible that drug binding broadens it beyond detection by the rR experiment.

DISCUSSION

Comparison of WT KatG and KatG(S315T) Heme Environments. Under equilibrium conditions, vibrational signatures of bound CO ligands in the KatG−CO adducts indicate two heme pocket conformations in both the WT and mutant enzymes. The positions of the enzymes on the ν(Fe−CO)/ν(C−O) back-bonding line in Figure 6 indicate a greater degree of back-bonding in form I than in form II. On this correlation line, form II of the KatG−COs is lower than Mb−CO, Hb−CO (*59*), and alkaline CCP−CO (*36*), whose vibrational signatures have been attributed to non-hydrogen-bonded Fe−CO units (Table 1). This suggests less interaction between the bound CO ligand and the distal heme pocket in form II than in form I, whose CO is H-bonded to a distal residue.

A higher fraction of form II is observed in KatG(S315T)−CO than in its WT counterpart. The lack of distal hydrogen bonding in form II is expected to impact the structural and electronic properties of the analogous O_2 complex. This could result in altered affinity of ferrous KatG(S315T) for O_2 and/or altered reactivity. If, as has been proposed (*31*, *35*), oxyKatG is a key heme intermediate in the INH activation mechanism, altered reactivity of this interediate due to the absence of distal hydrogen bonding could have a negative impact on the antitubercular potency of INH.

Sequence homology suggests that the distal histidines in HRP (His42) and CCP (His52) correspond to His108 in KatG. At pH 6.0 two CO conformers are observed for HRP−CO [ν(Fe−CO) 539 cm^{-1}, ν(C−O) 1906 cm^{-1} and ν(Fe−CO) 516 cm^{-1}, ν(C−O) 1934 cm^{-1}] (*36*, *38*, *46*, *60*). When the distal histidine is replaced with leucine [HRP(H42L)], only one CO conformer [ν(Fe−CO) 525 cm^{-1}, ν(C−O) 1924 cm^{-1}] is observed between pH 6 and pH 9.5 (*46*). The analogous CCP mutation yields a single form of CCP(H52L)−CO at pH 9.0 with ν(Fe−CO) at 522 cm^{-1} and ν(C−O) at 1928 cm^{-1} (*41*). Replacement of the distal His residues in HRP and CCP precludes the alkaline transition nomally observed at pH 8.3 for HRP−CO, implicating the distal His in the alkaline transition. A similar transition for either of the KatG−CO adducts would be expected to affect the equilibrium populations of forms I and II. The pH dependences of the WT KatG−CO and KatG(S315T)−CO rR spectra revealed no discernible pH dependence of the ν(Fe−CO) bands for forms I and II at $6 \leq$ pH ≤ 10 (data not shown.) Therefore, neither WT KatG−CO nor KatG-

(S315T)−CO undergoes an alkaline transition analogous to those observed for HRP and CCP. So it seems unlikely that the distal His108 participates in hydrogen bonding to the bound CO in WT KatG−CO or KatG(S315T)−CO (*46*).

Both HRP(H42L)−CO and CCP(H52L)−CO fall near form I of WT KatG−CO and KatG(S315T)−CO on the back-bonding correlation line, as seen in Figure 6. A proposed conformation of HRP(H42L)−CO has the oxygen of the CO hydrogen bonded through a water molecule to the guanidinium group of distal Arg38 (*46*). Since this Arg residue is conserved in KatG (Arg104) (*19*, *26*), an analogous Fe−CO−H_2O−Arg104 linkage between the heme iron and the distal pocket is proposed for form I of WT KatG−CO and KatG(S315T)−CO.

The low population of form I in the S315T enzyme suggests that either the position of the distal Arg104 side chain relative to the heme is perturbed by the methyl group of Thr315 or the bridging water molecule is extruded by a conformational reorganization of the WT heme pocket in response to S315T substitution. Indeed, KatG(R104L) mutated strains of *Mtb* are INH resistant (*61*), suggesting that Arg104 is crucial to INH activation. However, since strains with the distal His108 mutation KatG(H108Q) are also INH resistant (*61*), the loss of His108 hydrogen-bonding interactions could also be detrimental to INH activation. Sensitivity of the CO ligand vibrations to the seemingly innocuous S315T substitution near the heme periphery suggests that the native shape and rigidity of the distal heme pocket require most or all of the conserved heme pocket residues.

Effect of INH on WT and Mutant KatG Heme Environments. Intensity changes in the Raman bands attributed to the heme vinyl groups (Figure 1) indicate slight perturbation of the heme periphery upon treatment with INH. These small spectral changes are consistent with direct and/or indirect effects of INH mainly on the nonbonding interactions of the peripheral heme groups. This corroborates the conclusion from NMR T_1 measurements that INH binds in close proximity to the paramagnetic heme center (*32*, *33*). Minute changes in the ν_3 region of Figure 1 suggest that an INH-induced change in coordination number and/or spin state occurs in only a small fraction of the protein molecules at ambient temperature. This is consistent with previous optical and ESR studies wherein INH binding was investigated (*33*, *34*), all of which indicate a general insensitivity of the heme electronic properties to INH binding. Hence, although INH binds to both the WT and S315T enzymes, neither bonding nor strong nonbonding interactions between INH and the heme are likely. This argues for the protein structure and conformation around the heme being critical to forming a catalytically competent KatG−INH complex. Many of those structural and conformational features remain elusive at this time. However, the conformational properties of the heme and heme pocket that are sensitive to the presence of INH have been partially delineated in this study (vide infra).

Proximity of INH to the heme is further evidenced by low-temperature ESR spectra of ferric KatG that show partial conversion of the 6-c LS heme to HS upon INH bindng to WT KatG (*32*). It is possible to observe the INH-induced LS → HS conversion in ESR spectra because INH inhibits the freezing-induced shift in heme speciation from HS to LS, suggesting that INH diminishes the heme's affinity for one of the endogenous ligands (*34*). Thus, the ESR spectra also support the notion that INH binds close enough to the heme to influence the sixth ligand of a 6-c LS complex. Whether or not the actual interconversion of spin states and coordination numbers is physiologically relevant is not clear (*32*, *34*). Nevertheless, the observed interconversion does suggest that INH binding perturbs the conformation of the distal heme pocket. Previously reported NMR and ESR of the heme and the Fe−CO vibrations in WT and (S315T) CO adducts reported here are consistent with INH binding to both enzymes. Furthermore, they provide compelling evidence that it binds either inside or close enough to the distal heme pocket to influence the conformation of bound CO.

Comparisons of the low- and high-frequency Fe−C−O Raman intensities in Figure 8 reveal that when INH binds to WT KatG−CO, form I becomes predominant. This influence of INH on the population of form I is attenuated in KatG(S315T)−CO. Even though we were unable to observe the ν(C−O) band for INH-bound KatG(S315T)−CO, the low-frequency spectra show only a slight INH-induced increase in the population of form I (Figure 8). Given that oxyKatG(S315T) is about an order of magnitude less active than WT oxyKatG toward catalytic oxidation of INH (*31*), these results reveal a correlation between inability of KatG(S315T) to activate INH and its low population of the heme−CO form I conformation. This correlation supports the hypothesis that a form I analogue of the activating high-valent KatG intermediate is required for activation of INH. If oxyKatG is indeed the INH-activating intermediate, the diminished capacity of KatG(S315T) to supply a hydrogen-bonded form I analogue of oxyKatG could contribute to the mutant's inability to activate INH. Whether the hydrogen bond is required to poise the bound O_2 for further reduction and O−O bond cleavage or to allow INH to bind in an optimum orientation is not clear from the results reported here and will require further mechanistic study.

CONCLUSION

The data presented herein support several conclusions. Both the WT and S315T enzymes bind CO, and each is distributed between the two forms illustrated in Table 1. Form I of WT KatG−CO and KatG(S315T)−CO comprises a triatomic Fe−CO unit hydrogen bonded to a distal H donor. Possible donors include His108 or a water molecule bridged to Arg104. The position of form I on the back-bonding correlation plot suggests that the electrostatic environment of the hydrogen-bonded CO ligand is very similar to that in HRP and CCP mutants in which the distal His is replaced by Leu and CO is hydrogen bonded to the distal Arg through a water molecule. Since the diminished capacity of KatG(S315T) to supply form I does not appear to preclude INH binding, it probably compromises its ability to form the requisite intermediate heme species. Form I contains a neutral proximal imidazole (from His270, based on sequence homology with CCP). Form II also contains a neutral proximal imidazole ligand but has an Fe−CO unit that does not interact with distal residues through hydrogen bonding. While both WT and mutant enzymes have analogous CO conformers, form II with its less constrained Fe−CO moiety is more favored in KatG(S315T)−CO than in WT KatG−CO. Changes in relative Raman intensities of the ν(Fe−CO) bands upon treatment with INH show that drug binding perturbs bound CO in the distal pockets of both the WT and S315T

enzymes. In WT KatG−CO, INH binding increases the population of the hydrogen-bonded Fe−CO conformation (form I). Hence, it is reasonable to hypothesize that the inability of KatG(S315T) to activate INH (or activate enough INH) may derive from its inability to form sufficient amounts of hydrogen-bonded oxyKatG. Together with the compelling evidence for involvement of oxyKatG in INH activation, these observations suggest a necessity for hydrogen bonding between the distal heme pocket and a bound O_2 ligand for catalytic INH activation.

REFERENCES

1. World Health Organization (1998) World Health Report.
2. Mitchison, D. A. (1985) *Tubercle 66*, 219−225.
3. Stratton, M. A., and Reed, M. T. (1986) *Clin. Pharmacol. 5*, 977−987.
4. Riley, L. W. (1996) in *Tuberculosis* (Rom, W. N., and Gary, S., Eds.) pp 763−771, Little, Brown and Co., Boston, MA.
5. Moore, M., Onorato, I. M., McCray, E., and Castro, K. G. (1997) *JAMA, J. Am. Med. Assoc. 278*, 833−837.
6. Youatt J. (1961) *Aust. J. Chem. 14*, 308−311.
7. Mdluli, K., Swanson, J., Fisher, E., Lee, R. E., and Barry, C. E., III (1998) *Mol. Microbiol. 27*, 1223−1233.
8. Johnson, K., and Schultz, P. G. (1994) *J. Am. Chem. Soc. 116*, 7425−7426.
9. Banerjee, A., Dubnau, E., Quemard, A., Balasubramanian, V., Um, K. S., Wilson, T., Collins, D., deLisle, G., and Jacobs, W. R., Jr. (1994) *Science 263*, 227−230.
10. Quemard, A., Sacchettini, J. C., Dessen, A., Vilcheze, C., Bittman, R., Jacobs, W. R., Jr., and Blanchard, J. S. (1995) *Biochemistry 34*, 8235−8241.
11. Mdluli, K., Slayden, R. A., Zhu, Y., Ramaswamy, S., Pan, X., Mead, D., Crane, D. D., Musser, J. M., and Barry, C. E., III (1998) *Science 280*, 1607−1610.
12. Johnson, K., King, D. S., and Schultz, P. G. (1995) *J. Am. Chem. Soc. 117*, 5009−5010.
13. Quemard, A., Dressen, A., Sugantino, M., Jacobs, W. R., Jr., Sacchettini, J. C., and Blanchard, J. S. (1996) *J. Am. Chem. Soc. 118*, 1561−1562.
14. Basso, L. A., Zheng, R., and Blanchard, J. S. (1996) *J. Am. Chem. Soc. 118*, 11301−11302.
15. Basso, L. A., Zheng, R., Musser, J. M., Jacobs, W. R., Jr., and Blanchard, J. S. (1998) *J. Infect. Dis. 178*, 769−775.
16. Rozwarski, D. A., Grant, G. A., Barton, D. H. R., Jacobs, W. R., Jr., and Sacchettini, J. C. (1998) *Science 279*, 98−102.
17. Lei, B., Wei, C. J., and Tu, S. C. (2000) *J. Biol. Chem. 275*, 2520−2526.
18. Cockerill, F. R., III, Uhl, J. R., Temesgen, Z., Zhang, Y., Stockman, L., Roberts, G. D., Williams, D. L., and Kline, B. C. (1995) *J. Infect. Dis. 171*, 240−245.
19. Heym, B., Alzari, P. M., Honore, N., and Cole, S. T. (1995) *Mol. Microbiol. 15*, 235−245.
20. Musser, J. M., Kapur, V., Williams, D. L., Kreiswirth, B. N., van Soolingen, D., and van Embden, J. D. A. (1996) *J. Infect. Dis. 173*, 196−202.
21. Ramaswamy, S., and Musser, J. M. (1998) *Tubercle Lung Dis. 79*, 3−29.
22. Haas, W. H., Schilke, K., Brand, J., Amthor, B., Weyer, K., Fourie, P. B., Betzel, G., Sticht-Groh, V., and Bremer, H. J. (1997) *Antimicrob. Agents Chemother. 41*, 1601−1603.
23. Marttila, H. J., Soini, H., Eerola, E., Vyshnevakaya, E., Vyshnevskiy, B. I., Otten, T. F., Vasilyef, A. V., and Viljanen, M. K. (1998) *Antimicrob. Agents Chemother. 42*, 2443−2445.
24. Zhang, Y., Heym, B., Allen, B., Young, D., and Cole, S. (1992) *Nature 358*, 591−593.
25. Zhang, Y., Garbe, T., and Young, D. (1993) *Mol. Micorbiol. 8*, 521−524.
26. Heym, B., Zhang, Y., Poulet, S., Young, D., and Cole, S. T. (1993) *J. Bacteriol. 175*, 4255−4259.
27. Wengenack, N. L., Lopes, H., Kennedy, M. J., Tavares, P., Pereira, A. S., Moura, I., Moura, J. J. G., and Rusnak, F. (2000) *Biochemistry 39*, 11508−11513.
28. Wengenack, N. L., Uhl, J. R., St. Amand, A. L., Tomlinson, A. J., Benson, L. M., Naylor, S., Kline, B. C., Cockerill, F. R., III, and Rusnak, F. (1997) *J. Infect. Dis. 176*, 722−777.
29. Saint-Joanis, B., Souchon, H., Wilming, M., Johnsson, K., Alzari, P. M., and Cole, S. T. (1999) *Biochem. J. 338*, 753−760.
30. Chouchane, S., Lippai, I., and Magliozzo, R. S. (2000) *Biochemistry 39*, 9975−9983.
31. Wengenack, N. L., Hoard, H. M., and Rusnak, F. (1999) *J. Am. Chem. Soc. 121*, 9748−9749.
32. Todorovic, S., Juranic, N., Mucura, S., and Rusnak, F. (1999) *J. Am. Chem. Soc. 121*, 10962−10966.
33. Wengenack, N. L., Todorovic, S., Yu, L., and Rusnak, F. (1998) *Biochemistry 37*, 15825−15834.
34. Lukat-Rodgers, G. S., Wengenack, N. L., Rusnak, F., and Rodgers, K. R. (2000) *Biochemistry 39*, 9984−9993.
35. Magliozzo, R. S., and Marcinkeviciene, J. A. (1996) *J. Am. Chem. Soc. 118*, 11303−11304.
36. Evangelista-Kirkup, R., Smulevich, G., and Spiro, T. G. (1986) *Biochemistry 25*, 4420−4425.
37. Smulevich, G., Evangelista-Kirkup, R., English, A., and Spiro, T. G. (1986) *Biochemistry 25*, 4426−4431.
38. Uno, T., Nishimura, Y., Tsuboi, M., Makino, R., Iizuka, T., and Ishimura, Y. (1987) *J. Biol. Chem. 262*, 4549−4556.
39. Smulevich, G., Mauro, J. M., Fishel, L. A., English, A. M., Kraut, J., and Spiro, T. G. (1988) *Biochemistry 27*, 5486-5492.
40. Dasgupta, S., Rousseau, D. L., Anni, H., and Yonetani, T. (1989) *J. Biol. Chem. 264*, 654−662.
41. Smulevich, G., Miller, M. A., Kraut, J., and Spiro, T. G. (1991) *Biochemistry 30*, 9546−9558.
42. Oldfield, E., Guo, K., Augspurger, J. D., and Dykstra, C. E. (1991) *J. Am. Chem. Soc. 113*, 7537−7541.
43. Ray, G. B., Li, X., Ibers, J. A., Sessler, J. L., and Spiro, T. G. (1994) *J. Am. Chem. Soc. 116*, 162−176.
44. Holzbaur, I. E., English, A. M., and Ismail, A. A. (1996) *J. Am. Chem. Soc. 118*, 3354−3359.
45. Smulevich, G., Hu, S., Rodgers, K. R., Goodin, D. B., Smith, K. M., and Spiro, T. G. (1996) *Biospectroscopy 2*, 365−376.
46. Feis, A., Rodriguez-Lopez, J. N., Thorneley, R. N. F., and Smulevich, G. (1998) *Biochemistry 37*, 13575−13581.
47. Du, P., and Loew, G. H. (1991) *J. Phys. Chem. 95*, 6379−6383.
48. Boffi, A., Chiancone, E., Takahashi, S., and Rousseau, D. L (1997) *Biochemistry 36*, 4505−4509.
49. Kushkuley, B., and Stavrov, S. S. (1997) *Biochim. Biophys. Acta 1341*, 238−250.
50. Vogel, K. M., Kozlowski, P. M., Zgierski, M. Z., and Spiro, T. G. (1999) *J. Am. Chem. Soc. 121*, 9915−9921.
51. Bradford, M. M. (1976) *Anal. Biochem. 72*, 248−254.
52. Spiro, T. G., and Li, X. Y. (1988) in *Biological applications of Raman spectroscopy* (Spiro T. G., Ed.) Vol. 3, pp 1−37, John Wiley & Sons, New York.
53. Hu, S., Smith, K. M., and Spiro, T. G. (1996) *J. Am. Chem. Soc. 118*, 12638−12646.
54. Smulevich, G., Paoli, M., Burke, J. F., Sanders, S. A., Thorneley, R. N. F., and Smith A. T. (1994) *Biochemistry 33*, 7398−7407.
55. Marcinkeviciene, J. A., Magliozzo, R. S., and Blanchard J. S. (1995) *J. Biol. Chem. 270*, 22290−22295.
56. Vogel, K. M., Spiro, T. G., Shelver, D., Thorsteinsson, M. V., and Roberts, G. P. (1999) *Biochemistry 38*, 2679−2687.
57. Li, X. Y., and Spiro, T. G. (1988) *J. Am. Chem. Soc. 110*, 6024−6033.
58. Satterlee, J. D., and Erman, J. E. (1984) *J. Am. Chem. Soc. 106*, 1139−1140.
59. Tsubaki, M., Srivastava, R. V., and Yu, N. T. (1982) *Biochemistry 21*, 1132−1140.
60. Rodriguez-Lopez, J. N., George, S. J., and Thorneley, R. N. F. (1998) *J. Biol. Inorg. Chem. 3*, 44−52.
61. Rouse D. A., DeVito J. A., Li Z., Byer H., and Morris S. L. (1996) *Mol. Microbiol. 22*, 583−592.

BI010369G